

# Mutational signatures of DNA mismatch repair deficiency in *C. elegans* and human cancers

Bettina Meier,<sup>1,7</sup> Nadezda V. Volkova,<sup>2,7</sup> Ye Hong,<sup>1</sup> Pieta Schofield,<sup>1,3</sup>  
Peter J. Campbell,<sup>4,5,6</sup> Moritz Gerstung,<sup>2</sup> and Anton Gartner<sup>1</sup>

<sup>1</sup>Centre for Gene Regulation and Expression, University of Dundee, Dundee DD1 5EH, United Kingdom; <sup>2</sup>European Molecular Biology Laboratory, European Bioinformatics Institute (EMBL-EBI), Hinxton CB10 1SD, United Kingdom; <sup>3</sup>Division of Computational Biology, University of Dundee, Dundee DD1 5EH, United Kingdom; <sup>4</sup>Cancer Genome Project, Wellcome Trust Sanger Institute, Hinxton, Cambridge CB10 1SA, United Kingdom; <sup>5</sup>Department of Haematology, University of Cambridge, Cambridge CB2 0XY, United Kingdom; <sup>6</sup>Department of Haematology, Addenbrooke's Hospital, Cambridge CB2 0XY, United Kingdom

Throughout their lifetime, cells are subject to extrinsic and intrinsic mutational processes leaving behind characteristic signatures in the genome. DNA mismatch repair (MMR) deficiency leads to hypermutation and is found in different cancer types. Although it is possible to associate mutational signatures extracted from human cancers with possible mutational processes, the exact causation is often unknown. Here, we use *C. elegans* genome sequencing of *pms-2* and *mlh-1* knockouts to reveal the mutational patterns linked to *C. elegans* MMR deficiency and their dependency on endogenous replication errors and errors caused by deletion of the polymerase  $\epsilon$  subunit *pole-4*. Signature extraction from 215 human colorectal and 289 gastric adenocarcinomas revealed three MMR-associated signatures, one of which closely resembles the *C. elegans* MMR spectrum and strongly discriminates microsatellite stable and unstable tumors (AUC = 98%). A characteristic difference between human and *C. elegans* MMR deficiency is the lack of elevated levels of NCG > NTG mutations in *C. elegans*, likely caused by the absence of cytosine (CpG) methylation in worms. The other two human MMR signatures may reflect the interaction between MMR deficiency and other mutagenic processes, but their exact cause remains unknown. In summary, combining information from genetically defined models and cancer samples allows for better aligning mutational signatures to causal mutagenic processes.

[Supplemental material is available for this article.]

Cancer is a genetic disease associated with the accumulation of mutations. A major challenge is to understand mutagenic processes acting in cancer cells. Accurate DNA replication and the repair of DNA damage are important for genome maintenance. The identification of cancer predisposition syndromes caused by defects in DNA repair genes was important to link the etiology of cancer to increased mutagenesis. One of the first DNA repair pathways associated with cancer predisposition was DNA mismatch repair (MMR). MMR corrects mistakes that arise during DNA replication. Mutations in MMR genes are associated with hereditary nonpolyposis colorectal cancer (HNPCC), also referred to as Lynch Syndrome (Fishel et al. 1993; Bronner et al. 1994; Nicolaides et al. 1994; Papadopoulos et al. 1994; Miyaki et al. 1997).

DNA mismatch repair is initiated by the recognition of replication errors by MutS proteins, initially defined in bacteria. In *S. cerevisiae* and mammalian cells, two MutS complexes termed MutS $\alpha$  and MutS $\beta$ , comprised of MSH2/MSH6 and MSH2/MSH3 heterodimers, respectively, are required for DNA damage recognition albeit with differing substrate specificity (Drummond et al. 1995; Habraken et al. 1996; Genschel et al. 1998). Binding of MutS to the DNA lesion facilitates subsequent recruitment of the MutL complex. MutL enhances mismatch recognition and promotes a conformational change in MutS to allow for the sliding

of the MutL/MutS complex away from mismatched DNA (Allen et al. 1997; Gradia et al. 1999). DNA repair is initiated in most systems by a single-stranded nick generated by MutL (MutH in *E. coli*) on the nascent DNA strand at some distance to the lesion (Kadyrov et al. 2006, 2007). Exonucleolytic activities in part conferred by Exo1 contribute to the removal of the DNA stretch containing the mismatch followed by gap filling via lagging strand DNA synthesis (Goellner et al. 2015). The most prominent MutL activity in human cells is provided by the MutL $\alpha$  heterodimer MLH1/PMS2 (Prolla et al. 1998; Cannavo et al. 2005). Moreover, human MLH1 is found in heterodimers with PMS1 and MLH3, called MutL $\beta$  and MutL $\gamma$ . Of these, only MutL $\gamma$  is thought to have a minor role in MMR (Cannavo et al. 2005). The *C. elegans* genome does not encode obvious MutL $\beta$  and  $\gamma$  subunits (PMS1 and MLH3 homologs, respectively), whereas the MutL $\alpha$  subunits MLH-1 and PMS-2 can be readily identified using homology searches (Supplemental Table S1).

Analysis of mutations in microsatellite loci of *MLH1*-deficient colorectal cancer cell lines suggested rates of repeat expansion or contraction between  $8.4 \times 10^{-3}$  and  $3.8 \times 10^{-2}$  per locus and generation (Bhattacharyya et al. 1994; Hanford et al. 1998). Estimates using *S. cerevisiae* revealed a 100- to 700-fold increase in DNA repeat tract instability in *pms2*, *mlh1*, and *msh2* mutants (Strand et al. 1993) and an approximate fivefold increase in base substitution rates (Yang et al. 1999). *C. elegans* assays using reporter systems or selected, PCR-amplified regions revealed a >30-fold

<sup>7</sup>These authors contributed equally to this work.  
Corresponding authors: a.gartner@dundee.ac.uk,  
moritz.gerstung@ebi.ac.uk

Article published online before print. Article, supplemental material, and publication date are at <http://www.genome.org/cgi/doi/10.1101/gr.226845.117>. Freely available online through the *Genome Research* Open Access option.

© 2018 Meier et al. This article, published in *Genome Research*, is available under a Creative Commons License (Attribution 4.0 International), as described at <http://creativecommons.org/licenses/by/4.0/>.

increased frequency of single base substitutions in *msh-6*, a 500-fold increase in mutations in A/T homopolymer runs, and a 100-fold increase in mutations in dinucleotide repeats (Degtyareva et al. 2002; Tijsterman et al. 2002; Denver et al. 2005), akin to the frequencies observed in yeast and mammalian cells (Strand et al. 1993; Hanford et al. 1998). Recently, whole-genome sequencing approaches using diploid *S. cerevisiae* started to provide a genome-wide view of MMR deficiency. *S. cerevisiae* lines carrying an *msh2* deletion alone or in conjunction with point mutations in one of the three replicative polymerases—Pol $\alpha$ /primase, Pol $\delta$ , and Pole—were propagated over multiple generations to determine the individual contribution of replicative polymerases and MMR to replication fidelity (Lang et al. 2013; Lujan et al. 2014, 2015). These analyses estimated an average mutation rate of  $1.6 \times 10^{-8}$  per base pair per generation in *msh2* mutants and a further increased rate in double mutants of *msh2* and any of the replicative polymerases (Lujan et al. 2014, 2015). A synergistic increase in mutagenesis was also recently observed in childhood tumors in which MMR deficiency and mutations in replicative polymerase  $\epsilon$  and  $\delta$ , required for leading and lagging strand DNA synthesis, respectively, occurred (Shlien et al. 2015).

In human cancer samples, 30 mutational signatures (referred to as COSMIC signatures from here on) have been uncovered by mathematical modeling across a large number of cancer genomes representing more than 30 tumor types (<http://cancer.sanger.ac.uk/cosmic/signatures>) (Alexandrov et al. 2013a,b). These signatures are largely defined by the relative frequency of the six possible base substitutions (C>A, C>G, C>T, T>A, T>C, and T>G) in the sequence context of their adjacent 5' and 3' base. Of these, COSMIC signatures 6, 15, 20, 21, and 26 have been associated with MMR deficiency with several MMR signatures being present in the same tumor sample (Alexandrov et al. 2013a,b). It is not clear whether these MMR signatures are conserved across evolution and how they reflect MMR defects. Therefore, MMR signatures deduced from defined monogenic MMR-defective backgrounds (which we will herein refer to as mutational patterns) could contribute to the refinement of computationally derived mutational signatures extracted from cancer genomes.

Here, we investigate the genome-wide mutational impact of the loss of the MutL mismatch repair genes *mlh-1* and *pms-2* in the nematode *C. elegans*. Furthermore, we address the contribution of a deletion of *pole-4*, a nonessential accessory subunit of the leading-strand DNA polymerase Pole, to mutation profiles and hypermutation.

## Results

### Mutation rates and profiles of *mlh-1*, *pms-2*, and *pole-4* single mutants grown over 20 generations

We previously established *C. elegans* mutation accumulation assays and demonstrated that defects in major DNA damage response and DNA repair pathways, including nucleotide excision repair, base excision repair, DNA crosslink repair, DNA end-joining, and apoptosis, did not lead to overtly increased mutation rates when lines were propagated for 20 generations (Meier et al. 2014). The experimental setup takes advantage of the 3–4 d life cycle of *C. elegans* and its hermaphroditic reproduction by self-fertilization. This allows for the propagation of clonal *C. elegans* lines, which in each generation pass through a single-cell bottleneck provided by the zygote. We now extend these studies to MMR deficiency conferred by MutL $\alpha$  mutations *mlh-1* and *pms-2*. Because null al-

leles of the human and *C. elegans* leading-strand polymerase Pole catalytic subunit, *POLE* and *pole-1*, respectively, cause lethality, we focused our analysis on a nonessential *C. elegans* Pole subunit, termed POLE-4. Dbp3p, the *S. cerevisiae* POLE-4 ortholog, has been implicated in stabilizing POLE interaction with the primer-template DNA complex (Aksenova et al. 2010).

We detected an average of four base substitutions and two insertions/deletions in wild-type *C. elegans* lines propagated for 20 generations (Fig. 1A,B). In contrast, *mlh-1* and *pms-2* mismatch repair single mutants carried an average of 1174 and 1191 unique mutations, respectively, of which 288 and 309 were base substitutions (Fig. 1A) and 886 and 882 indels, defined as small insertions and deletions of <400 bp (Fig. 1B). The nature of single nucleotide changes and the overall mutation burden were congruent across independent lines of the same genotype, and mutation numbers linearly increased from F10 to F20 generation lines (Fig. 1). In contrast to *mlh-1* and *pms-2*, *pole-4* mutants exhibited mutation numbers and profiles not significantly different from wild-type (Fig. 1; Supplemental Table S2).

### Mutation rates and patterns in *pole-4*; *pms-2* double mutants

To further investigate the role of *pole-4* and the genetic interaction with MMR deficiency, we generated *pole-4*; *pms-2* double mutants. *pms-2* mutants carried an average of 145 base substitution and 527 indels over 10 generations, roughly half the number we observed in the F20 generation (Fig. 1C,D; Supplemental Table S2). In comparison, the number of single base substitutions and indels was increased ~4.4-fold and ~1.4-fold in *pole-4*; *pms-2* double mutants to an average of 637 and 723, respectively (Fig. 1C,D; Supplemental Table S2). We did not identify any structural variants (SVs) in the genotypes analyzed except for *pole-4*, in which a single SV was observed in three F10 mutation accumulation lines (Supplemental Table S2). We could not readily propagate *pole-4*; *pms-2* beyond the F10 generation, suggesting that a mutation burden higher than ~500–700 single base substitutions (Fig. 1C) in conjunction with 700–750 indels (Fig. 1D) might be incompatible with organismal reproduction. The increased mutation burden of *pole-4*; *pms-2* double mutants compared to that of *pms-2* and to the wild-type mutation rate of *pole-4* suggests that replication errors occur at increased frequency in the absence of *pole-4* but are effectively repaired by MMR.

Assuming that it takes 15 cell divisions to go through the *C. elegans* life cycle and considering that heterozygous mutations can be lost during self-fertilization (Methods), we calculated a mutation rate per base pair and germ cell division of  $1.0 \times 10^{-9}$  (95% CI:  $7.96 \times 10^{-10}$  to  $1.25 \times 10^{-9}$ ) for wild-type and  $1.19 \times 10^{-9}$  (95% CI:  $9.58 \times 10^{-10}$  to  $1.45 \times 10^{-9}$ ) for *pole-4* mutants. In contrast, mutation rates for *mlh-1* and *pms-2* were  $7.10 \times 10^{-8}$  (95% CI:  $6.86 \times 10^{-8}$  to  $7.33 \times 10^{-8}$ ) and  $7.28 \times 10^{-8}$  (95% CI:  $7.10 \times 10^{-8}$  to  $7.48 \times 10^{-8}$ ), respectively. *pole-4*; *pms-2* double mutants exhibited a mutation rate of  $1.51 \times 10^{-7}$  (95% CI:  $1.45 \times 10^{-7}$  to  $1.56 \times 10^{-7}$ ).

The genome-wide mutation rates observed in the absence of *C. elegans* MutL $\alpha$  proteins MLH-1 and PMS-2 are in line with mutation rates previously determined for *C. elegans* MutS and *S. cerevisiae* MMR mutants (Strand et al. 1993; Yang et al. 1999; Degtyareva et al. 2002; Tijsterman et al. 2002; Denver et al. 2005). However, unlike in mammalian cells (Yao et al. 1999; Baross-Francis et al. 2001), *C. elegans* *mlh-1* and *pms-2* mutants exhibited almost identical mutation rates and profiles, suggesting that the inactivation of the MutL $\alpha$  heterodimer is sufficient to

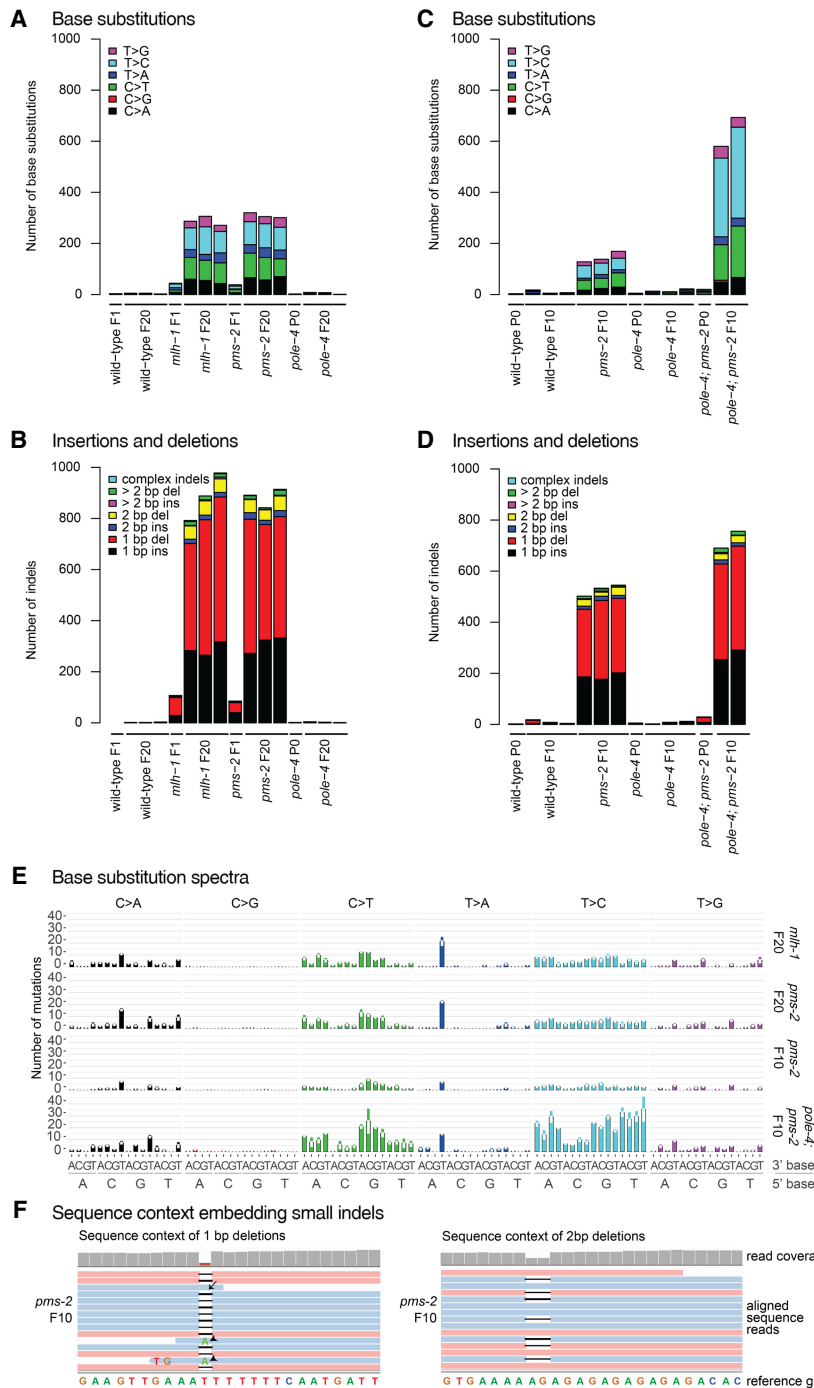


**Figure 1.** Mutations in *C. elegans* wild-type and MMR mutants grown for 10 or 20 generations. Identical base substitutions as well as indels occurring in the same genomic location among samples of the entire data set (duplicates) were excluded from the analysis, thus only reporting mutations unique to each individual sample. (A) Number and types of base substitutions identified in the parental (P0) or one first generation (F1) line and three independently propagated F20 lines of wild-type, *mlh-1*, *pms-2*, and *pole-4* single mutants. (B) Number and types of insertions and deletions (indels) identified in initial (P0 or F1) and three independently propagated F20 lines of wild-type, *mlh-1*, *pms-2*, and *pole-4* single mutants. (C) Number and types of base substitutions observed in the parental (P0) line and 2–3 independently propagated F10 lines of wild-type, *pms-2* and *pole-4* single, and *pole-4*; *pms-2* double mutants. (D) Number and type of indels observed in the parental (P0) and 2–3 independently propagated F10 lines of wild-type, *pms-2* and *pole-4* single, and *pole-4*; *pms-2* double mutants. (E) Average number of base substitutions identified across all individual lines per genotype in their 5' and 3' base sequence context in *mlh-1* and *pms-2* single and in *pms-2* single and *pole-4*; *pms-2* double mutants. Error bars represent the standard error of the mean. (F) Examples of indel sequence contexts. Sequence reads aligned to the reference genome WBcel235.74 visualized in Integrative Genomics Viewer (Robinson et al. 2011). A 1-bp (left) and a 2-bp deletion (right) are shown. A subset of sequence reads, which end close to an indel, erroneously aligned across the indel resulting either in wild-type bases (arrow) or base changes (arrowheads). Such wrongly called base substitutions were removed during filtering (Methods) using the deepSNV package (Gerstung et al. 2012, 2014).

induce a fully penetrant MMR phenotype consistent with the absence of PMS1 MutL $\beta$  and MLH3 MutL $\gamma$  homologs in *C. elegans*. Our finding that *pole-4* mutants do not show increased mutation rates is surprising given that the deletion of the budding yeast *pole-4* homolog *DPB3* leads to mutation rates comparable to the proofreading-deficient *pol2-4* allele of the Pole catalytic subunit (Aksenova et al. 2010; Lujan et al. 2012). Increased mutation rates have also been reported for proofreading mutants of the Pole catalytic subunit in mice and human, and in humans such mutations are associated with an increased predisposition to colorectal cancer (Albertson et al. 2009; Lujan et al. 2012; Palles et al. 2013).

### Distribution and sequence context of base substitutions

We next wished to determine the mutational patterns associated with DNA mismatch repair defects alone and combined with *pole-4* deficiency. T>C and C>T transitions were present more frequently than T>A, T>G, C>A, and C>G transversions in *mlh-1* and *pms-2* single and *pole-4*; *pms-2* double mutants (Fig. 1A,C; Supplemental Table S2). A similar preponderance of T>C and C>T transitions was previously observed in *S. cerevisiae* *msh2* mutants and in MMR-defective human cancer lines (Alexandrov et al. 2013a; Lujan et al. 2014; Supek and Lehner 2015). Analyzing all base substitutions within their 5' and 3' sequence context, we found no prominent enrichment of distinct 5' and 3' bases associated with T>C transitions in *mlh-1* and *pms-2* single mutants. In contrast, T>A transversions occurred with increased frequency in an ATT context, C>T transitions in a GCN context, and C>A transversions in a NCT context (Fig. 1E).

Interestingly, >90% of T>A transversions in homopolymer runs; the majority (>75%) in the context of two adjoining A and T homopolymers (Supplemental Fig. S1A). An increased frequency of base substitution at the junction of adjacent repeats has also been reported in *S. cerevisiae* MMR mutants, giving rise to the speculation that such base substitutions may be generated by double slippage events (Lang et al. 2013). Moreover, we observed several examples in which one or several base substitutions had occurred that converted a repeat sequence such that it

became identical to flanking repeats consistent with polymerase slippage across an entire repeat (Supplemental Fig. S1B–D). Such mechanisms could lead to the equalization of microsatellite repeats, a phenomenon referred to as microsatellite purification (Harr et al. 2000).

Although we could not define mutational patterns specifically associated with *pole-4* loss due to the low number of mutations, the profile of *pole-4; pms-2* double mutants differed from MMR single mutants. In addition to C>T transitions in a G<sub>C</sub>N context, T>C transitions were generated with higher frequency, accounting for >50% of all base changes (Fig. 1C). Among these, T>C substitutions in the context of a flanking 5' cytosine were underrepresented (Fig. 1E). A higher proportion of T>C changes, not embedded in a defined sequence context, has been reported for MMR-deficient tumor samples containing mutations in the lagging strand polymerase Pol $\delta$  (Shlien et al. 2015), but not in *S. cerevisiae*

and human tumors with a combined MMR and Pole deficiency (Lujan et al. 2014; Shlien et al. 2015). No obvious chromosomal clustering of base substitutions was observed in *pms-2* and *pole-4; pms-2* grown for 10 generations (Supplemental Fig. S2A).

### Sequence context of insertions and deletions associated with MMR deficiency

The majority of mutations observed in *mlh-1* and *pms-2* single and *pole-4; pms-2* double mutants were small insertions/deletions (indels) (Fig. 1B,D). Of these, ~90% constituted 1-bp indels (Fig. 1B,D; Supplemental Table S2) with most 1-bp indels occurring in homopolymer runs (Figs. 1F, 2B). On average, 2-bp indels accounted for 5.5%–8.6% of indels observed (Fig. 1B,D; Supplemental Table S2) and affected dinucleotide repeat sequences (Fig. 1F) and homopolymer runs at similar frequency, as recently also

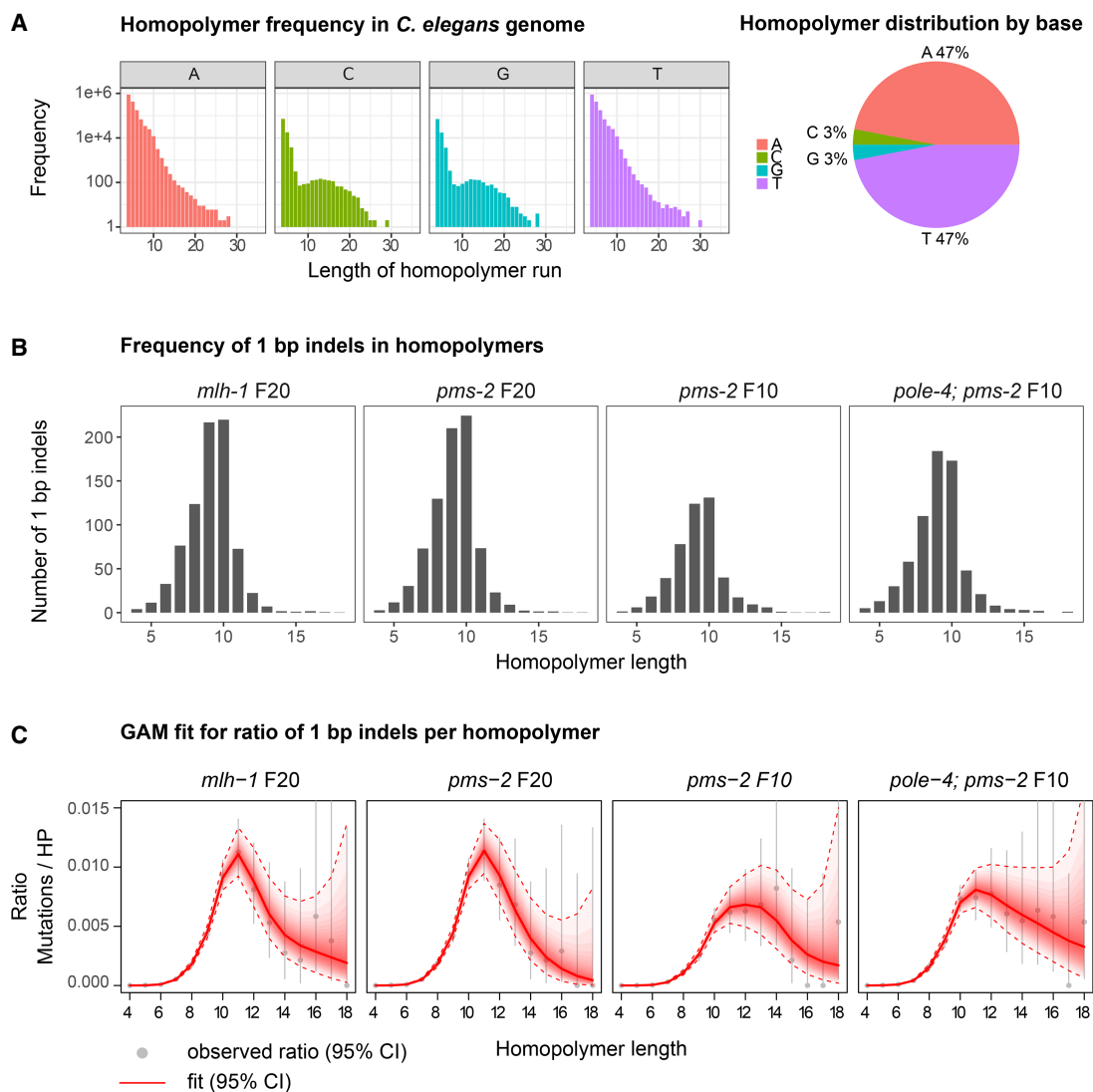


**Figure 2.** Correlation between homopolymer length and the frequency of +1/–1 bp indels. (A) Distribution of homopolymer repeats encoded in the *C. elegans* genome by length and DNA base shown in log<sub>10</sub> scale (left) and the relative percentage of A, C, G, and T homopolymers in the genome (right). (B) Average number of 1-bp indels in homopolymer runs for *mlh-1* F20, *pms-2* F20, *pms-2* F10, and *pole-4; pms-2* F10 mutant lines by homopolymer length. (C) Generalized additive spline model (GAM) fit for the ratio of 1-bp indels normalized to the frequency of homopolymers (HPs) in the genome. The average frequency observed across three lines is depicted as a gray dot; gray bars indicate the 95% confidence interval. The red line indicates best fit. Red dotted lines represent the corresponding 95% confidence interval.

reported for MMR mutants in *S. cerevisiae* (Lujan et al. 2015). Trinucleotide repeat instability is associated with a number of neurodegenerative disorders, such as fragile X syndrome, Huntington's disease, and Spinocerebellar Ataxias (Brouwer et al. 2009). Based on our analysis, trinucleotide repeat sequences are present in the *C. elegans* genome at a >400-fold lower frequency than homopolymer runs (Methods; Supplemental Data Analysis). We observed between three and seven trinucleotide indels per 10 generations in *mlh-1* and *pms-2* mutants (Supplemental Table S2). However, these occurred predominantly in homopolymer sequences precluding an estimation of mutation rates for trinucleotide repeats.

Clustering of 1-bp indels was not evident for *pms-2* and *pole-4*; *pms-2*F10 lines beyond a somewhat reduced occurrence in the center of *C. elegans* autosomes, which correlates with reduced homopolymer frequency in these regions (Supplemental Fig. S2B).

### Dependency of 1-bp indel frequency on homopolymer length

Given the high number of indels present in homopolymer repeats, we aimed to investigate the correlation between indel frequency and homopolymer length. Overall, we identified 3,433,785 homopolymers in the *C. elegans* genome, ranging in length between 4 and 35 nt (Fig. 2A; Methods). Of all homopolymers, 47% each were poly(A) or poly(T) repeats, their frequencies decreasing with increasing length (Fig. 2A). C and G each comprised 3% of all homopolymers with frequencies decreasing up to a length of 8 bp, plateauing between 8 and 17 bp, and further decreasing for longer homopolymer tracts (Fig. 2A). These findings are consistent with a previous report on homopolymers >7 bp long (Denver et al. 2004). In *C. elegans* MMR mutant backgrounds, the frequency of 1-bp indels increased with homopolymer length of up to 9–10 bp and trailed off in longer homopolymers (Fig. 2B). Because the frequency of homopolymer tracts decreases with length (Fig. 2A), we normalized for homopolymer number. To incorporate the uncertainty of the frequency estimation, we applied an additive model (Methods), which supported our findings of a rapid increase in indel frequency in homopolymers up to a repeat length of 10 bases, followed by a drop or plateau in indel frequency for longer homopolymers with decreasing confidence (Fig. 2C). Firm conclusions about indel frequencies in homopolymers >13 bp are precluded by the lack of statistical power due to the low numbers of both long homopolymers in the genome and associated indels observed (Fig. 2A,B). In summary, our data suggest that replicative polymerase slippage occurs more frequently with increasing homopolymer length, with a peak for homopolymers of 10–11 nt, followed by reduced slippage frequency in longer homopolymers. These results are consistent with observations in budding yeast (Lang et al. 2013) and a recent study using human *MLH1* KO organoids (Drost et al. 2017).

### Comparison of *C. elegans* MMR patterns to MMR signatures derived from human colorectal and gastric adenocarcinoma samples

To assess how our findings relate to mutation profiles occurring in human cancer, we analyzed whole-exome sequencing data from the TCGA colorectal adenocarcinoma project COAD-US (<http://icgc.org/icgc/cgp/73/509/1134>) (The Cancer Genome Atlas Network 2012) and the TCGA gastric adenocarcinoma project STAD-US (<https://icgc.org/icgc/cgp/69/509/70268>) (The Cancer Genome Atlas Research Network 2014). These cancer types are commonly associated with MMR deficiency. These data sets con-

tain single nucleotide (SNV) and indel variant calls from 215 and 289 donors, respectively. Having observed high 1-bp indel frequencies associated with homopolymer repeats in *C. elegans pms-2* and *mlh-1* mutants (Figs. 1B,D, 2B), we also considered indels in our analysis of human mutational signatures.

A *t*-distributed stochastic neighbor embedding (*t*-SNE) representation of the cosine similarities of mutation spectra revealed a distinctive grouping of cancer samples (Fig. 3A; Methods). De novo signature extraction across both tumor cohorts combined revealed eight main mutational signatures (Fig. 3B; Methods). Comparing these to existing COSMIC signatures by calculating the similarity score between their base substitution profiles showed that many had a counterpart in the COSMIC database with high similarity (Table 1; Supplemental Fig. S3B), validating our results. We labeled three of the de novo signatures as “MMR-1–3.” MMR-1 shares similarity with COSMIC signature 20, MMR-2 with COSMIC signature 15, and MMR-3 with COSMIC signatures 21 and 26 (Table 1; Supplemental Fig. S3B).

One signature identified in the tumor samples showed characteristics of *POLE* mutations (“POLE”; <http://cancer.sanger.ac.uk/cosmic/signatures>) (Fig. 3B; Supplemental Fig. S3B; Alexandrov et al. 2013a). C > T mutations in a CpG base context result from 5mC deamination and are referred to as “Clock-1” (Fig. 3B; Supplemental Fig. S3B). “Clock-2” is present in the majority of samples and likely reflects background mutation rates (Fig. 3A,B). Signature “17-like” is of unknown etiology, predominantly found in stomach cancers, and related to COSMIC signature 17 (Fig. 3B; Supplemental Fig. S3B). Finally, we identified a signature indicative of SNP contamination characterized by a high overlap of somatic mutations with SNPs present in the human population and a lower nonsynonymous to synonymous ratio, as expected for germline variants (Fig. 3B; Supplemental Material).

To confirm the link between signatures MMR-1–3 and mismatch repair deficiency, we correlated their occurrence with the microsatellite stability status of samples according to the Stanford TCGA Clinical Explorer (<http://genomeportal.stanford.edu/pan-tcga>).

We considered the samples with microsatellite instable-high (MSI-H) status as MMR-deficient and refer to them as microsatellite instable (MSI), whereas microsatellite instable-low (MSI-L) and microsatellite stable (MSS) samples are considered MMR-proficient and referred to as MSS. In the COAD cohort, 40 of the 215 (19%) samples, and in the STAD, 63 of the 289 (22%) samples were assigned MSI status. Comparing MSI/MMR-deficient and MSS/MMR-proficient samples, we found that the fraction of MMR-1, MMR-2, and MMR-3 signatures was strongly enriched in a cluster of microsatellite instable cancer samples (Wilcoxon rank-sum test *P*-values  $1.7 \times 10^{-51}$ ,  $2.7 \times 10^{-22}$ , and  $9.8 \times 10^{-29}$ , respectively) (Fig. 3A, top left, 3C). Consistent with the results from *C. elegans*, 82% of indels in the human cancer samples were 1-bp insertions or deletions (25,093 and 30,561 in COAD and STAD cohort, respectively). The majority of these occurred in homopolymer runs at frequencies ranging between 69% and 72% in COAD and 91% and 93% in STAD samples (Supplemental Fig. S4B). Of all signatures identified, only MMR-1 highly correlated with the amount of 1-bp indels (Pearson correlation coefficient of 0.99), showing a stable trend compared to other MMR signatures (Fig. 3B,D). MMR-1 signature contribution was a remarkably accurate indicator of MSI/MMR deficiency (AUC of 0.98, 95% confidence interval [CI] 0.97–1).

Individual signatures often represent the most extremes of the mutational spectrum; a typical tumor, however, is usually represented by a linear combination of multiple processes. In the

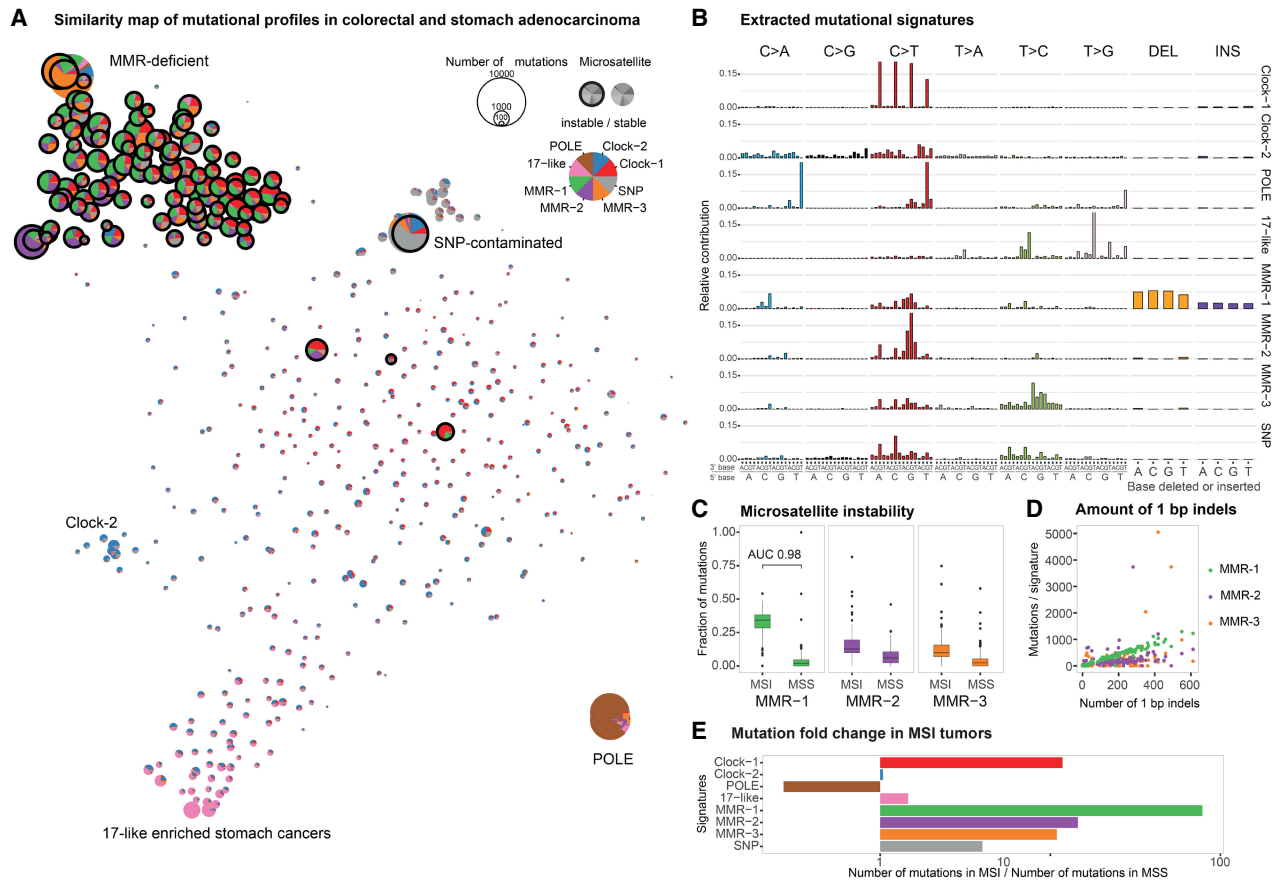


**Figure 3.** Identification of de novo signatures from human colorectal and gastric adenocarcinoma samples (COAD-US and STAD-US projects) and their contribution to samples clinically classified as microsatellite unstable (MSI) or microsatellite stable (MSS). (A) Two-dimensional representation of the mutational profile composition across cancer samples. The size of each circle reflects the mutation burden. MSI samples are highlighted by a bold, black outline. The color of segments reflects the signature composition. (B) Mutational signatures including base substitutions and 1-bp indels derived from the combined COAD-US and STAD-US data sets. (C) Relative contribution of MMR-1, MMR-2, and MMR-3 signatures to cancer samples clinically classified as MSI or MSS. Box plot with outliers shown as individual filled circles. Area under the curve (AUC) value for MMR-1 contribution indicates the probability of a random MSI sample having higher MMR-1 contribution than a random MSS sample. (D) Number of mutations assigned to signatures MMR-1 (green), MMR-2 (purple), and MMR-3 (orange) plotted against the number of 1-bp indels in the same sample. As expected, the number of POLE-related mutations is higher in MSS samples as all POLE-deficient tumors are MSS. Apart from MMR signatures, Clock-1 signature also contributes over 10 times more mutations to MSI samples than to MSS. SNP associated mutations are likely due to unfiltered SNPs that are prevalent in the human population (Supplemental Material).

cluster of MSI-H tumors (Fig. 3A, top left) MMR-1 occurs with high relative contribution in the majority of MSI-H tumors, whereas MMR-2 and MMR-3 contributions are generally smaller and more variable across these tumors (Fig. 3A; Supplemental Fig. S5A,B). However, the most severely hypermutated samples are largely described by a single signature (Fig. 3A, MMR-2 in purple, MMR-3 in orange). Minor contributions of MMR-2 and MMR-3 in other tumors may be due to the tendency of the signature calculation method to extract signatures predominantly from the most extreme cases and imparting them on other samples. We considered that MMR-2 and MMR-3 might reflect different substrate specificities of MMR complexes arising from an inactivation of unique subunits of MutS $\alpha$ , MutS $\beta$ , MutL $\alpha$ , or MutL $\gamma$  heterodimers. Investigating MMR gene mutations and methylation status in MSI tumor samples, we only observed few cases of *MSH6* (MutS $\alpha$ ), *MSH3* (MutS $\beta$ ), *PMS2* (MutL $\alpha$ ), *PMS1* (MutL $\beta$ ), and *MLH3* (MutL $\gamma$ ) high-impact mutations often in combination with inactivation of other MMR genes (Supplemental Material; Supplemental Table S3). We observed an increased number of mu-

tations assigned to the Clock-1 signature in human MMR-deficient samples (Fig. 3A,E). The Clock-1/COSMIC signature 1 is thought to reflect spontaneous 5mC deamination and its conversion to thymine, a mutational process that is thought to be active in all tissues and that correlates with the age at the time of cancer diagnosis (Alexandrov et al. 2013a). Our data suggest a role of MMR in the repair of 5mC deamination-induced mismatches (Bellacosa 2001; Tricarico et al. 2015; Grin and Ishchenko 2016). Notably the most frequent MMR-associated COSMIC signature, Signature 6, shows high rates of C > T mutations in an NCG context possibly reflecting imperfect delineation of the underlying mutational processes.

A second sample cluster is represented by six tumors (Fig. 3A, bottom right) with most of their mutations falling within the POLE signature (brown). Consistently, these samples also carry pathogenic *POLE* mutations (Supplemental Table S4). Another cluster is formed by a subset of stomach cancer samples carrying a 17-like signature (Fig. 3A, bottom left). Four tumor samples outside of these clusters and dispersed over the similarity map are MSI. These tumors may have acquired MMR deficiency very late in their development.

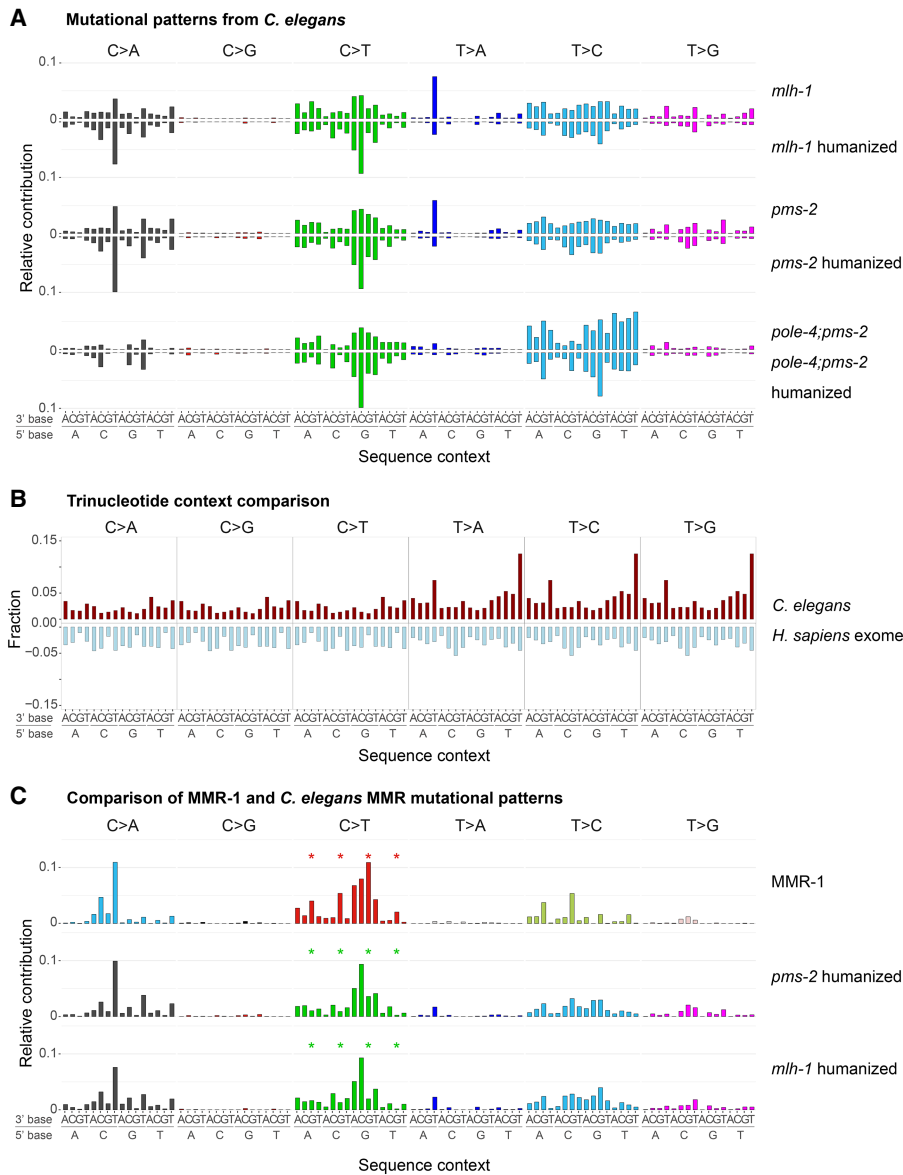


**Figure 4.** Mutational patterns derived from *C. elegans* MMR mutants and their comparison to the de novo human signature MMR-1. (A) Base substitution patterns of *C. elegans* *mlh-1*, *pms-2*, and *pole-4;pms-2* mutants and their corresponding humanized versions (mirrored). (B) Relative abundance of trinucleotides in the *C. elegans* genome (red) and the human exome (light blue). (C) MMR-1 base substitution signature compared to *pms-2* and *mlh-1* mutational patterns adjusted to human whole-exome trinucleotide frequency. Stars indicate the difference in C>T transitions at CpG sites, which occur at lower frequency in *C. elegans*.

To compare human and *C. elegans* MMR footprints, we first determined mutational patterns from *mlh-1* and *pms-2* single mutants as well as from the *pole-4;pms-2* double mutant (Methods). Mutational patterns of *mlh-1* and *pms-2* mutants were nearly identical with a cosine similarity of 0.97 (Fig. 4A, top panels). In contrast the *pole-4;pms-2* mutational pattern showed a different relative contribution of C>T and T>C mutations (Fig. 4A, top panels) and displayed a cosine similarity to *mlh-1* and *pms-2* below 0.71 (Supplemental Fig. S6C). We next adjusted for the difference in trinucleotide frequencies in the *C. elegans* genome and the human exome (Fig. 4A, bottom panels, 4B). Comparison of *C. elegans* MMR patterns with known cancer signatures showed the highest

similarity of 0.77 to COSMIC signature 20 (Table 1; Supplemental Fig. S7). Of the three human MMR-associated de novo signatures, only MMR-1 displayed similarity to *C. elegans* MMR substitution patterns with a cosine similarity of 0.84 to *pms-2* and of 0.81 to *mlh-1* (Table 1; Fig. 4C). A notable difference in the *C. elegans* *pms-2* and *mlh-1* patterns compared to the MMR-1 signature are a reduced level of C>T mutations in NCG contexts (Fig. 4C, stars) and a high frequency of T>A mutation in an ATT context. The first is likely due to the lack of spontaneous deamination of 5methyl-C, a base modification that is absent in *C. elegans* (Greer et al. 2015); the latter is likely due to a higher relative frequency of poly(A) and poly(T) homopolymers in the *C. elegans* genome versus the human exome (Fig. 2A; Supplemental Fig. S4A). Excluding C>Ts in NCG contexts from the analysis increases the cosine similarity of MMR-1 up to 0.92 for *pms-2* and up to 0.90 for *mlh-1* patterns and reduces the uncertainty in similarity scores (Supplemental Material; Supplemental Fig. S6D). The similarity between *C. elegans* MMR and the human MMR-1 mutational footprints is further supported by the concurrent presence of a large number of 1-bp indels. None of the human signatures showed notable similarity to the *pole-4;pms-2* mutation pattern.

### Discussion

MMR-deficient tumors have among the highest mutation rates across cancer types. In line with this observation, we observed a dramatic increase in base substitutions and indels in *C. elegans* *mlh-1* and *pms-2* mutants. This mutation rate is only surpassed by that of the *pole-4;pms-2* double mutant in which mutation rates are further increased two- to three-fold. Genome maintenance is highly efficient as evidenced by a wild-type *C. elegans* mutation rate in the order of  $8 \times 10^{-10}$  per base and cell division. It thus

appears that DNA repair pathways act highly redundantly, and it may require the combined deficiency of multiple DNA repair pathways to trigger excessive mutagenesis. Equally, a latent defect in DNA replication integrity might only become apparent in conjunction with a DNA repair deficiency. Indeed the increased mutation burden detected in the *pole-4;pms-2* double mutant, while no increased mutation rate is observed in *pole-4* alone, uncovers a latent role of *pole-4*. It appears that replication errors occur at increased frequency in the absence of *C. elegans* *pole-4* but are effectively repaired by MMR.

Out of the signatures associated with MMR deficiency in cancer cells, only MMR-1 is related to the mutational pattern found in

**Table 1.** Cosine similarity values for the comparison between humanized *C. elegans* derived MMR mutation patterns with human de novo signatures and selected COSMIC signatures (both adjusted to human whole-exome trinucleotide frequencies)

				COSMIC signatures											
				1	2	3	5	6	10	15	17	20	21	26	
				<i>mlh-1</i>	0.28	0.09	0.56	0.71	0.44	0.16	0.44	0.27	0.77	0.56	0.63
				<i>pms-2</i>	0.28	0.09	0.53	0.68	0.48	0.18	0.50	0.25	0.77	0.48	0.61
				<i>pole-4; pms-2</i>	0.26	0.12	0.45	0.68	0.40	0.13	0.50	0.17	0.56	0.69	0.74
				<i>C. elegans</i> patterns											
				<i>mlh-1</i>											
				<i>pms-2</i>											
				<i>pole-4;</i>											
				<i>pms-2</i>											
De novo signatures	Clock 1	0.18	0.17	0.15	0.98	0.11	0.14	0.53	0.86	0.36	0.52	0.20	0.53	0.42	0.46
	Clock 2	0.36	0.32	0.30	0.24	0.62	0.75	0.66	0.18	0.13	0.12	0.19	0.31	0.19	0.27
	POLE	0.19	0.21	0.15	0.32	0.26	0.19	0.31	0.24	0.97	0.18	0.18	0.24	0.17	0.23
	17-like	0.23	0.21	0.13	0.06	0.04	0.22	0.26	0.08	0.06	0.06	0.98	0.12	0.12	0.20
	MMR-1	0.81	0.85	0.63	0.59	0.08	0.43	0.71	0.79	0.24	0.70	0.20	0.85	0.43	0.65
	MMR-2	0.36	0.43	0.42	0.67	0.04	0.14	0.49	0.86	0.21	0.99	0.12	0.30	0.22	0.49
	MMR-3	0.62	0.56	0.75	0.39	0.09	0.34	0.62	0.42	0.16	0.35	0.18	0.53	0.95	0.91
	SNP	0.52	0.47	0.55	0.73	0.14	0.48	0.83	0.69	0.25	0.38	0.29	0.79	0.63	0.71

*C. elegans mlh-1* and *pms-2* mutants. Considering the controlled nature of the *C. elegans* experiment, we postulate that MMR-1 reflects a conserved mutational process of DNA replication repaired by MMR. Consistent with this, we find that MMR-1 activity is closely linked to MSI status, an established indicator for mismatch repair deficiency. In cases of hypermutation, we suggest that akin to the *pole-4; pms-2* double mutant, mutational footprints can be attributed to the failed repair of lesions originating from mutations in DNA repair or DNA replication genes. For instance, in MMR-defective lines also carrying *POLE* catalytic subunit mutations, the mutational landscape is overwhelmed by the *POLE* signature (Shlien et al. 2015). Likewise it appears possible that the MMR-2 and MMR-3 signatures could be attributed to other mutational processes, which are repaired by MMR and lead to hypermutation under MMR deficiency. Overall, MMR-1 seemingly reflects a “basal” mutational process in both humans and *C. elegans*. In addition, human MMR deficiency also includes an element of failing to repair lesions arising from CpG deamination and leading to C > T mutations, a process absent in *C. elegans* due to the lack of cytosine methylation. The associated human signature, “Clock-1,” together with MMR-1 explains the majority of mutations occurring in MMR-defective cancers not apparently affected by hypermutation.

Matching mutational signatures to DNA repair deficiency has a tremendous potential to stratify cancer therapy tailored to DNA repair deficiency. This approach appears advantageous over genotyping marker genes, as mutational signatures provide a read-out for cellular repair deficiency associated with either genetic or epigenetic defects. Following on from our study, we expect that analyzing DNA repair-defective model organisms and human cell lines, alone or in conjunction with defined genotoxic agents, will contribute to a more precise definition of mutational signatures occurring in cancer genomes and to establishing the etiology of these signatures.

## Methods

### *C. elegans* maintenance and propagation

*C. elegans* mutants *pole-4(tm4613) II*, *pms-2(ok2529) V*, and *mlh-1(ok1917) III* were backcrossed six times against the wild-type N2 reference strain TG1813 (Meier et al. 2014). *pole-4 II*; *pms-2 V* double mutants were generated as described in Supplemental Material. Strains were grown for 10 or 20 generations, and genomic DNA was prepared as described (Supplemental Material; Meier et al. 2014).

### DNA sequencing, variant calling, and post-processing

Illumina sequencing, variant calling, and post-processing filters were performed as described (Meier et al. 2014) with the following adjustments. WBcel235.74.dna.toplevel.fa was used as the reference genome ([http://ftp.ensembl.org/pub/release-74/fasta/caenorhabditis\\_elegans/dna/](http://ftp.ensembl.org/pub/release-74/fasta/caenorhabditis_elegans/dna/)). Alignments were performed with BWA-MEM, and mutations were called using CaVEMan, Pindel, and BRASSII (Ye et al. 2009; Stephens et al. 2012), each available at <https://github.com/cancerit>. Post-processing of mutation calls was performed across a large data set of 2202 sequenced samples using filter conditions as described (Supplemental Material; Meier et al. 2014). An additional filtering step using deepSNV (<https://bioconductor.org/packages/release/bioc/html/deepSNV.html>) was used to correct for wrongly called base substitutions, events due to algorithm-based sequence misalignment of ends of sequence reads covering 1-bp indels (Fig. 1F).

### Estimating mutation rates

Mutation rates were calculated using maximum likelihood methods, assuming 15 cell divisions per generation (Meier et al. 2014) and considering that mutations have a 25% chance to be lost, a 50% chance to be transmitted as heterozygous, and a 25% chance to become homozygous, thus becoming fixed in the line during each round of *C. elegans* self-fertilization. Wild-type, *pole-4*, and *pms-2* mutation rates were calculated from mutations observed across F10 and F20 generations.

### Analysis of homopolymer sequences in *C. elegans* and human cancer samples

Homopolymers, dinucleotide, and trinucleotide runs encoded in the *C. elegans* genome, defined here as repetitive DNA regions with a consecutive number of identical bases or repeated sequence of  $n \geq 4$ , were identified from the reference genome WBcel235.74 using an in-house script (Supplemental Data Analysis Scripts; <https://github.com/gerstung-lab/MMR>) based on R packages Biostrings (<http://www.bioconductor.org/packages//2.7/bioc/html/Biostrings.html>, R package version 2.42.2) and GenomicRanges (<https://bioconductor.org/packages/release/bioc/html/GenomicRanges.html>). Overall, 3,433,785 homopolymers, 25,126 dinucleotide, and 7615 trinucleotide repeats were identified. Matching the genomic position of 1-bp indels observed in *pms-2* and *pole-4; pms-2* mutants to the genomic positions of homopolymers, we defined 1-bp indels present in homopolymer runs and the length of the homopolymer in which they occurred.



Generalized additive models with a spline term were used to correlate the frequency of 1-bp indels occurring in homopolymer runs with the frequency of the respective homopolymer in the *C. elegans* genome. An average of ~0.5 1-bp indels arising in homopolymer sequences was observed in 101 wild-type lines of different generations, indicating the frequency with which such events might occur in wild-type or as amplification artifacts during sequencing (Supplemental Material). Consistent with COAD and STAD variant calling, homopolymer frequencies and coordinates in the human exome were calculated based on the GRCh37 human reference genome build and the coordinates of well-covered fractions of whole-exome sequencing regions as reported by Agilent SureSelect V5 Human All Exon (<https://earray.chem.agilent.com/earray/>). Overall, we identified 976,390 homopolymers in the human exome, which ranged from 4 to 35 bp in length (Supplemental Fig. S4A). A more recent genome build, GRCh38, does not differ in the composition of coding regions. Therefore the analysis of homopolymer frequencies is valid using both assembly versions.

### De novo signature extraction from human cancer samples

Variant calls for whole-exome sequencing data from the colorectal adenocarcinoma (COAD-US) and gastric adenocarcinoma (STAD-US) projects were taken from the ICGC database (<http://icgc.org>). Mutational counts and contexts were inferred from variant tables using MutationalPatterns R package (<http://bioconductor.org/packages/release/bioc/html/MutationalPatterns.html>). After combining indels and substitutions into vectors of length 104, we extracted the signatures using the Brunet NMF with KL-divergence as implemented in Blokzijl et al. (2016), which is equivalent to a Poisson NMF model. The number of signatures was determined based on the saturation of both the Akaike Information Criterion (AIC) (Akaike 1973) and the residual sum of squares (RSS) (Supplemental Fig. S3A; Supplemental Material).

Similarity between signatures was calculated via cosine similarity as follows:

$$\text{similarity}(S_1, S_2) = \frac{\langle S_1, S_2 \rangle}{\|S_1\| \cdot \|S_2\|},$$

where  $\langle S_1, S_2 \rangle$  is a scalar product of signature vectors. When compared to 96-long substitution signatures, indels were omitted from 104-long de novo signatures.

Stochastic nearest neighbor representation (*t*-SNE) (van der Maaten and Hinton 2008) was obtained using R package “tsne” (<https://cran.r-project.org/web/packages/tsne/tsne.pdf>) using the cosine similarity as distance measure between mutational profiles. In order to confirm the link between signatures MMR-1–3 and MMR deficiency, we defined MMR-deficient samples as those annotated as MSI-H (microsatellite instable-high) in TCGA Clinical Explorer (Lee et al. 2015). Relative contributions of every signature to the samples from the combined data set were tested for association with MSI/MSS status using one-tailed Wilcoxon rank-sum test. All *P*-values were adjusted for multiple testing correction using the Bonferroni procedure.

### Comparison of *C. elegans* mismatch repair mutation patterns to cancer signatures

To extract the signatures of individual factors from respective *C. elegans* samples, we used additive Poisson model with multiple factors for every trinucleotide context and indel type and calculated maximum likelihood estimates for every signature (Supplemental Material). For comparison of *C. elegans* and human mutational signatures, signatures acquired in *C. elegans* were adjusted by multiplying the probability for 96 base substitutions by

the ratio of respective trinucleotide counts observed in the human exome (GRCh37) counts precalculated in Rosenthal et al. (2016) to those in the *C. elegans* reference genome (WBcel235). Indels were not included in the comparative analysis as they required adjustment for both base and homopolymer content. COSMIC signatures were also adjusted to exome nucleotide counts, because they were mostly derived from whole exomes (Alexandrov et al. 2013a,b) and the comparison of de novo signatures to COSMIC is more valid in exome space. All signatures were further normalized so that the vector of probabilities sums up to 1 (Supplemental Table S5). For mutational signature comparison, a cosine similarity of 0.80 was considered a threshold for “high” similarity (Supplemental Material; Supplemental Fig. S6A,B).

### Data analysis

R scripts (R Core Team 2017) used to analyze *C. elegans* and cancer data sets are available in Supplemental Data Analysis Scripts and on GitHub under <https://github.com/gerstung-lab/MMR>.

### Data access

Sequencing data from this study have been submitted to the NCBI Sequence Read Archive (SRA; <http://www.ncbi.nlm.nih.gov/sra>) under accession number SRP020555.

### Acknowledgments

This work was supported by a Wellcome Trust Senior Research award to A.G. (090944/Z/09/Z) and by a Wellcome Trust Strategic Award (101126/B/13/Z). B.M., N.V.V., P.J.C., M.G., and A.G. are members of the Wellcome Trust funded COMSIG (Causes of Mutational SIGNatures) consortium. P.S. and the Data Analysis Group, Dundee, were funded by the “Wellcome Trust Technology Platform” Strategic Award 097945/Z/11/Z. We thank the Mitani laboratory funded by the National Bio-Resource Project, Japan, and the Caenorhabditis Genetics Center funded by the NIH Office of Research Infrastructure Programs (P40 OD010440) for providing strains. We also thank Steve Hubbard, University of Dundee, for help with statistics.

### References

- Akaike H. 1973. Information theory and an extension of the maximum likelihood principle. In *2nd International symposium of information theory*, pp. 267–281, Akademiai Kiado, Budapest.
- Aksenova A, Volkov K, Maceluch J, Pursell ZF, Rogozin IB, Kunkel TA, Pavlov YI, Johansson E. 2010. Mismatch repair-independent increase in spontaneous mutagenesis in yeast lacking non-essential subunits of DNA polymerase  $\epsilon$ . *PLoS Genet* **6**: e1001209.
- Albertson TM, Ogawa M, Bugni JM, Hays LE, Chen Y, Wang Y, Treuting PM, Heddle JA, Goldsby RE, Preston BD. 2009. DNA polymerase  $\epsilon$  and  $\delta$  proofreading suppress discrete mutator and cancer phenotypes in mice. *Proc Natl Acad Sci* **106**: 17101–17104.
- Alexandrov LB, Nik-Zainal S, Wedge DC, Aparicio SA, Behjati S, Biankin AV, Bignell GR, Bolli N, Borg A, Børresen-Dale AL, et al. 2013a. Signatures of mutational processes in human cancer. *Nature* **500**: 415–421.
- Alexandrov LB, Nik-Zainal S, Wedge DC, Campbell PJ, Stratton MR. 2013b. Deciphering signatures of mutational processes operative in human cancer. *Cell Rep* **3**: 246–259.
- Allen DJ, Makhov A, Grilley M, Taylor J, Thresher R, Modrich P, Griffith JD. 1997. MutS mediates heteroduplex loop formation by a translocation mechanism. *EMBO J* **16**: 4467–4476.
- Barros-Francis A, Makhani N, Liskay RM, Jirik FR. 2001. Elevated mutant frequencies and increased C:G→T:A transitions in *Mlh1*<sup>-/-</sup> versus *Pms2*<sup>-/-</sup> murine small intestinal epithelial cells. *Oncogene* **20**: 619–625.
- Bellacosa A. 2001. Functional interactions and signaling properties of mammalian DNA mismatch repair proteins. *Cell Death Differ* **8**: 1076–1092.

- Bhattacharyya NP, Skandalis A, Ganesh A, Groden J, Meuth M. 1994. Mutator phenotypes in human colorectal carcinoma cell lines. *Proc Natl Acad Sci* **91**: 6319–6323.
- Blokzijl F, Janssen R, Van Boxtel R, Cuppen E. 2016. MutationalPatterns: an integrative R package for studying patterns in base substitution catalogues. bioRxiv doi: 10.1101/071761.
- Bronner CE, Baker SM, Morrison PT, Warren G, Smith LG, Lescoe MK, Kane M, Earabino C, Lipford J, Lindblom A, et al. 1994. Mutation in the DNA mismatch repair gene homologue *hMLH1* is associated with hereditary non-polyposis colon cancer. *Nature* **368**: 258–261.
- Brouwer JR, Willemsen R, Oostra BA. 2009. Microsatellite repeat instability and neurological disease. *Bioessays* **31**: 71–83.
- The Cancer Genome Atlas Network. 2012. Comprehensive molecular characterization of human colon and rectal cancer. *Nature* **487**: 330–337.
- The Cancer Genome Atlas Research Network. 2014. Comprehensive molecular characterization of gastric adenocarcinoma. *Nature* **513**: 202–209.
- Cannavo E, Marra G, Sabates-Bellver J, Menigatti M, Lipkin SM, Fischer F, Cejka P, Jiricny J. 2005. Expression of the MutL homologue hMLH3 in human cells and its role in DNA mismatch repair. *Cancer Res* **65**: 10759–10766.
- Degtyareva NP, Greenwell P, Hofmann ER, Hengartner MO, Zhang L, Culotti JG, Petes TD. 2002. *Caenorhabditis elegans* DNA mismatch repair gene *msh-2* is required for microsatellite stability and maintenance of genome integrity. *Proc Natl Acad Sci* **99**: 2158–2163.
- Denver DR, Morris K, Kewalramani A, Harris KE, Chow A, Estes S, Lynch M, Thomas WK. 2004. Abundance, distribution, and mutation rates of homopolymeric nucleotide runs in the genome of *Caenorhabditis elegans*. *J Mol Evol* **58**: 584–595.
- Denver DR, Feinberg S, Estes S, Thomas WK, Lynch M. 2005. Mutation rates, spectra and hotspots in mismatch repair-deficient *Caenorhabditis elegans*. *Genetics* **170**: 107–113.
- Drost J, van Boxtel R, Blokzijl F, Mizutani T, Sasaki N, Sasselli V, de Ligt J, Behjati S, Grolleman JE, van Wezel T, et al. 2017. Use of CRISPR-modified human stem cell organoids to study the origin of mutational signatures in cancer. *Science* **358**: 234–238.
- Drummond JT, Li GM, Longley MJ, Modrich P. 1995. Isolation of an hMSH2-p160 heterodimer that restores DNA mismatch repair to tumor cells. *Science* **268**: 1909–1912.
- Fishel R, Lescoe MK, Rao MR, Copeland NG, Jenkins NA, Garber J, Kane M, Kolodner R. 1993. The human mutator gene homolog *MSH2* and its association with hereditary nonpolyposis colon cancer. *Cell* **75**: 1027–1038.
- Genschel J, Littman SJ, Drummond JT, Modrich P. 1998. Isolation of MutS $\beta$  from human cells and comparison of the mismatch repair specificities of MutS $\beta$  and MutS $\alpha$ . *J Biol Chem* **273**: 19895–19901.
- Gerstung M, Beisel C, Rechsteiner M, Wild P, Schraml P, Moch H, Beerwinkel N. 2012. Reliable detection of subclonal single-nucleotide variants in tumour cell populations. *Nat Commun* **3**: 811.
- Gerstung M, Papaemmanuil E, Campbell PJ. 2014. Subclonal variant calling with multiple samples and prior knowledge. *Bioinformatics* **30**: 1198–1204.
- Goellner EM, Putnam CD, Kolodner RD. 2015. Exonuclease 1-dependent and independent mismatch repair. *DNA Repair* **32**: 24–32.
- Gradia S, Subramanian D, Wilson T, Acharya S, Makhov A, Griffith J, Fishel R. 1999. hMSH2-hMSH6 forms a hydrolysis-independent sliding clamp on mismatched DNA. *Mol Cell* **3**: 255–261.
- Greer EL, Blanco MA, Gu L, Sendinc E, Liu J, Aristizábal-Corrales D, Hsu CH, Aravind L, He C, Shi Y. 2015. DNA methylation on N<sup>6</sup>-adenine in *C. elegans*. *Cell* **161**: 868–878.
- Grin I, Ishchenko AA. 2016. An interplay of the base excision repair and mismatch repair pathways in active DNA demethylation. *Nucleic Acids Res* **44**: 3713–3727.
- Habraken Y, Sung P, Prakash L, Prakash S. 1996. Binding of insertion/deletion DNA mismatches by the heterodimer of yeast mismatch repair proteins MSH2 and MSH3. *Curr Biol* **6**: 1185–1187.
- Hanford MG, Rushton BC, Gown LC, Farber RA. 1998. Microsatellite mutation rates in cancer cell lines deficient or proficient in mismatch repair. *Oncogene* **16**: 2389–2393.
- Harr B, Zangerl B, Schlötterer C. 2000. Removal of microsatellite interruptions by DNA replication slippage: phylogenetic evidence from *Drosophila*. *Mol Biol Evol* **17**: 1001–1009.
- Kadyrov FA, Dzantiev L, Constantin N, Modrich P. 2006. Endonucleolytic function of MutL $\alpha$  in human mismatch repair. *Cell* **126**: 297–308.
- Kadyrov FA, Holmes SF, Arana ME, Lukianova OA, O'Donnell M, Kunkel TA, Modrich P. 2007. *Saccharomyces cerevisiae* MutL $\alpha$  is a mismatch repair endonuclease. *J Biol Chem* **282**: 37181–37190.
- Lang GL, Parsons L, Gammie AE. 2013. Mutation rates, spectra, and genome-wide distribution of spontaneous mutations in mismatch repair deficient yeast. *G3* **3**: 1453–1465.
- Lawrence M, Huber W, Pagès H, Aboyoun P, Carlson M, Gentleman R, Morgan MT, Carey VJ. 2013. Software for computing and annotating genomic ranges. *PLoS Comput Biol* **9**: e1003118.
- Lee H, Palm J, Grimes SM, Ji HP. 2015. The Cancer Genome Atlas Clinical Explorer: a web and mobile interface for identifying clinical-genomic driver associations. *Genome Med* **7**: 112.
- Lujan SA, Williams JS, Pursell ZF, Abdulovic-Cui AA, Clark AB, Nick McElhinny SA, Kunkel TA. 2012. Mismatch repair balances leading and lagging strand DNA replication fidelity. *PLoS Genet* **8**: e1003016.
- Lujan SA, Clausen AR, Clark AB, MacAlpine HK, MacAlpine DM, Malc EP, Mieczkowski PA, Burkholder AB, Fargo DC, Gordenin DA, et al. 2014. Heterogeneous polymerase fidelity and mismatch repair bias genome variation and composition. *Genome Res* **24**: 1751–1764.
- Lujan SA, Clark AB, Kunkel TA. 2015. Differences in genome-wide repeat sequence instability conferred by proofreading and mismatch repair defects. *Nucleic Acids Res* **43**: 4067–4074.
- Meier B, Cooke SL, Weiss J, Bailly AP, Alexandrov LB, Marshall J, Raine K, Maddison M, Anderson E, Stratton MR, et al. 2014. *C. elegans* whole-genome sequencing reveals mutational signatures related to carcinogens and DNA repair deficiency. *Genome Res* **24**: 1624–1636.
- Miyaki M, Konishi M, Tanaka K, Kikuchi-Yanoshita R, Muraoka M, Yasuno M, Igari T, Koike M, Chiba M, Mori T. 1997. Germline mutation of *MSH6* as the cause of hereditary nonpolyposis colorectal cancer. *Nat Genet* **17**: 271–272.
- Nicolaides NC, Papadopoulos N, Liu B, Wei YF, Carter KC, Ruben SM, Rosen CA, Haseltine WA, Fleischmann RD, Fraser CM, et al. 1994. Mutations of two PMS homologues in hereditary nonpolyposis colon cancer. *Nature* **371**: 75–80.
- Palles C, Cazier JB, Howarth KM, Domingo E, Jones AM, Broderick P, Kemp Z, Spain SL, Guarino E, Salguero I, et al. 2013. Germline mutations affecting the proofreading domains of POLE and POLD1 predispose to colorectal adenomas and carcinomas. *Nat Genet* **45**: 136–144.
- Papadopoulos N, Nicolaides NC, Wei YF, Ruben SM, Carter KC, Rosen CA, Haseltine WA, Fleischmann RD, Fraser CM, Adams MD, et al. 1994. Mutation of a mutL homolog in hereditary colon cancer. *Science* **263**: 1625–1629.
- Prolla TA, Baker SM, Harris AC, Tsao JL, Yao X, Bronner CE, Zheng B, Gordon M, Reneker J, Arnheim N, et al. 1998. Tumour susceptibility and spontaneous mutation in mice deficient in Mlh1, Pms1 and Pms2 DNA mismatch repair. *Nat Genet* **18**: 276–279.
- R Core Team. 2017. *R: a language and environment for statistical computing*. R Foundation for Statistical Computing, Vienna, Austria. <https://www.R-project.org/>.
- Robinson JT, Thorvaldsdóttir H, Winckler W, Guttman M, Lander ES, Getz G, Mesirov JP. 2011. Integrative genomics viewer. *Nat Biotechnol* **29**: 24–26.
- Rosenthal R, McGranahan N, Herrero J, Taylor BS, Swanton C. 2016. deconstructSigs: Delineating mutational processes in single tumors distinguishes DNA repair deficiencies and patterns of carcinoma evolution. *Genome Biol* **17**: 31.
- Shlien A, Campbell BB, de Borja R, Alexandrov LB, Merico D, Wedge D, Van Loo P, Tarpey PS, Coupland P, Behjati S, et al. 2015. Combined hereditary and somatic mutations of replication error repair genes result in rapid onset of ultra-hypermutated cancers. *Nat Genet* **47**: 257–262.
- Stephens PJ, Tarpey PS, Davies H, Van Loo P, Greenman C, Wedge DC, Niker-Zainal S, Martin S, Varela I, Bignell GR, et al. 2012. The landscape of cancer genes and mutational processes in breast cancer. *Nature* **486**: 400–404.
- Strand M, Prolla TA, Liskay RM, Petes TD. 1993. Destabilization of tracts of simple repetitive DNA in yeast by mutations affecting DNA mismatch repair. *Nature* **365**: 274–276.
- Supek F, Lehner B. 2015. Differential DNA mismatch repair underlies mutation rate variation across the human genome. *Nature* **521**: 81–84.
- Tijsterman M, Pothof J, Plasterk RH. 2002. Frequent germline mutations and somatic repeat instability in DNA mismatch-repair-deficient *Caenorhabditis elegans*. *Genetics* **161**: 651–660.
- Tricarico R, Cortellino S, Riccio A, Jagmohan-Changur S, Van der Klift H, Wijnen J, Turner D, Ventura A, Rovella V, Percepe A, et al. 2015. Involvement of *MBD4* inactivation in mismatch repair-deficient tumorigenesis. *Oncotarget* **6**: 42892–42904.
- van der Maaten L, Hinton G. 2008. Visualizing high-dimensional data using t-SNE. *J Mach Learn Res* **9**: 2579–2605.
- Yang Y, Karthikeyan R, Mack SE, Vonarx EJ, Kunz BA. 1999. Analysis of yeast *pms1*, *msh2*, and *mlh1* mutators points to differences in mismatch correction efficiencies between prokaryotic and eukaryotic cells. *Mol Gen Genet* **261**: 777–787.
- Yao X, Buermeier AB, Narayanan L, Tran D, Baker SM, Prolla TA, Glazer PM, Liskay RM, Arnheim N. 1999. Different mutator phenotypes in *Mlh1*-versus *Pms2*-deficient mice. *Proc Natl Acad Sci* **96**: 6850–6855.
- Ye K, Schulz MH, Long Q, Apweiler R, Ning Z. 2009. Pindel: a pattern growth approach to detect break points of large deletions and medium sized insertions from paired-end short reads. *Bioinformatics* **25**: 2865–2871.

Received June 27, 2017; accepted in revised form January 2, 2018.